**PAPER • OPEN ACCESS**

# Optofluidic liquid sensing on electromicrofluidic devices

To cite this article: Manuel Oliva-Ramírez *et al* 2020 *Mater. Res. Express* **7** 036407

View the article online for updates and enhancements.

## You may also like

- A compact and portable optofluidic device for detection of liquid properties and label-free sensing
  F Lahoz, I R Martín, D Walo et al.

- Optofluidics based lab-on-chip device for *in situ* measurement of mean droplet size and droplet size distribution of an emulsion
  P K Shivhare, A Prabhakar and A K Sen

- Optofluidic multi-measurement system for the online monitoring of lubricant oil
  Tom Verschooten, Manly Callewaert, Leonardo Ciaccheri et al.

# Materials Research Express

# Optofluidic liquid sensing on electromicrofluidic devices

Manuel Oliva-Ramírez[1,2] , Siang-Lin Wang[3], Víctor Rico-Gavira[1] , Carmen López-Santos[1], Shih-Kang Fan[4] and Agustín R González-Elipe[1]

1   Instituto de Ciencia de Materiales de Sevilla (CSIC-Univ. Sevilla), Avda. Américo Vespucio 49, 41092 Sevilla, Spain
2   Department of Materials for Electronics and Electrical Engineering, Institute of Materials Science and Engineering and Institute of Micro- and Nanotechnologies MacroNano®, TU Ilmenau, D-98693 Ilmenau, Germany
3   Department of Mechanical Engineering, National Taiwan University, Taipei, Taiwan
4   Department of Mechanical and Nuclear Engineering, Kansas State University, Manhattan, KS 66506, United States of America

**E-mail:** manuel.oliva-ramirez@tu-ilmenau.de

## Abstract

Electromicrofluidic (EMF) devices are used to handle and move tiny amounts of liquids by electrical actuation, including electrowetting-on-dielectric (EWOD) and dielectrophoresis (DEP). Monitoring the liquid characteristics in one of these devices requires suitable sensing transducers incorporated within the microfluidic structure. In the present work, we describe the incorporation of an optofluidic photonic transducer in an EMF device to monitor the refractive index of a liquid during its manipulation. The incorporated transducer consists of a responsive porous Bragg Microcavity (BM) deposited via physical vapor oblique angle deposition. Besides reporting the manufacturing procedure of the sensing-EMF device combining liquid handling and monitoring, the performance of the BM is verified by infiltrating several liquids dripped on its surface and comparing the responses with those of liquid droplets electrically moved from the delivery part of the chip to the BM location. This study proved that modified EMF devices can incorporate photonic structures to analyze very low liquid volumes ($\sim$0.2 $\mu$L) during its handling.

## 1. Introduction

Measuring the Refractive Index (RI) of a liquid sample is one of the most common biological/chemical analysis methods using optofluidic sensors. Although this method only reveals differences in liquids with different RI, the availability of procedures relying on a microfluidic approach (i.e., handling minute amounts of liquid) may be of interest for certain niche applications (e.g., to monitor solute concentration in solutions or mixture of liquids) where the scarcity of samples is a bottleneck for a conventional RI detection [1]. Optofluidic RI sensors based on plasmonics [2–6], photonic crystals [7–11] or photonic crystals fibers [12] are primarily composed of periodic metallic or dielectric structures that can be used to confine and guide light. However, even if these sensing techniques enable detection of liquids with extremely small volumes, in practice, the rudimentary character of the currently available liquid delivery systems makes that still relatively large liquid volumes are required for detection. Not to mention the difficulty of selectively and precisely positioning various analytes at the detection spot where the light–matter interaction is the strongest [13].

Microfluidic devices offer a wide variety of methods for handling small amounts of liquids in a controlled way. The so-called electromicrofluidic (EMF) method, operating by changing the interfacial properties of the driven liquids using electric forces, e.g., electrowetting-on-dielectric (EWOD) and dielectrophoresis (DEP), is one of the most popular and successful procedures to generate and move droplets on an array of electrostatically actuated electrodes [14–19]. EMF offers precise and programmable liquid positioning and is more reliable than other microfluidics procedures. It consumes very little power and is easily scalable [20]. Moreover, an EMF platform is ideal for accommodating and incorporating complex sensing modules. In recent years, EMF systems have been used for biosensing applications that provide high throughputs of the parallel processing of multiple samples on a single chip. Several works have already demonstrated the potential use of EMF devices for liquid

handling [21–29] and sensing [30]. In particular, EMF devices integrating optical refractive index procedures, such as surface plasmon resonance [31, 32] and microrings [33–35], have been applied with promising results. However, these systems usually involve time-consuming and expensive fabrication methods, which call for more practical alternatives. In the present work we prove the feasibility of a new and simple approach to incorporate a RI detecting sensor to a EMF device. The easiness of the preparation method, its solventloss character and its compatibility with any kind of substrate, including polymers, make this approach very interesting to incorporate of a miniaturized optofluidic sensor onto a selected part of the EMF chip. Moreover, the reported experiments prove that the selective deposition of the sensor BM does not affect the electrical response of the EMF chip.

The procedure relies on a recently reported results about the manufacturing by physical vapor oblique angle deposition (PV-OAD) [36–38] of porous multilayers in the form of Bragg Microcavities (BMs). This system consists of the successive stacking of porous layers of two transparent materials with different refractive indices and was successfully tested for the detection of glucose solutions. Due to light interference processes, the optical spectra of these multilayers present a resonant peak in the middle of a band gap that can be used for monitoring the refractive index of liquids or solutions filling the pores. An outstanding characteristic of these porous BMs as optofluidic sensor device is their capacity to monitor very low analyte volumes (~1 nL) [36–38]. The present work constitutes an attempt to combine in a single chip system with an EMF device for handling small droplets of liquids and with a porous BM chip, thus providing the double capacity of moving liquids at the microscale and proceeding to their RI analysis. For this purpose, we firstly describe the fabrication of a porous BM onto an EMF chip. Secondly, we prove that the thus modified EFM chip retained its capacity of moving liquids between their driving electrodes. Finally, to test the performance of this system, we compare the optofluidic response of the BM incorporated in the EMF device electrically actuated with EWOD or DEP forces to move the liquid droplet till the measurement point with the measurements of liquids manually dripped onto the BM surface. The equivalent results obtained in the two cases prove the feasibility of the approach to integrate in a single chip the capacity to move liquid droplet and to proceed to their analysis in an electrically operated way.

## 2. Experimental methods

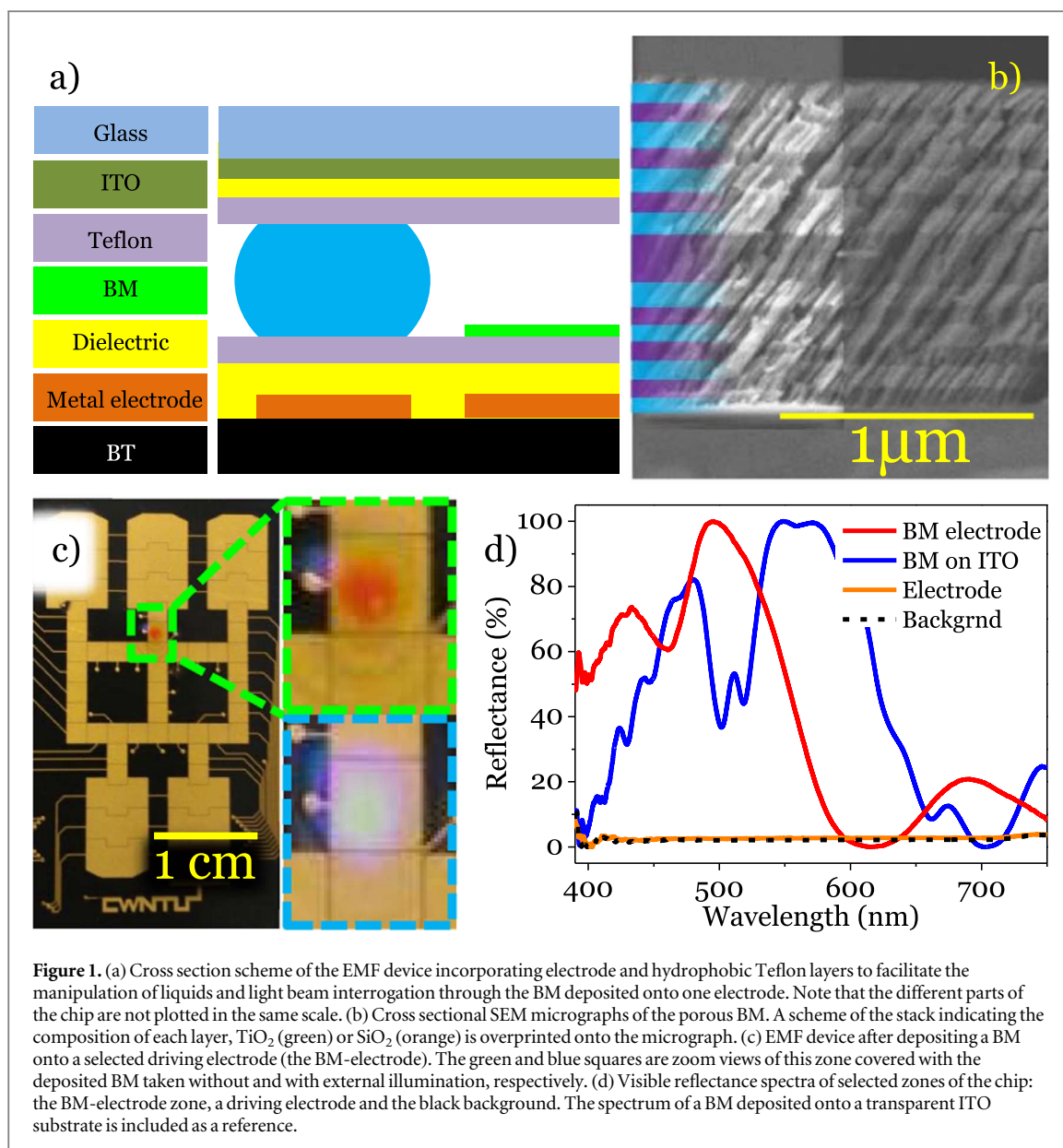### 2.1. Electromicrofluidic device preparation

Figure 1(a) shows that the EMF device consists of two parallel plates with an unpatterned ground electrode on the top plate, the patterned driving electrode on the bottom plate and a spacer of 50 $\mu$m between them. We used a top glass plate (thickness 0.7 mm) coated with transparent indium tin oxide [39] (ITO, thickness 200 nm) to enable optical analyses and direct observation during the experiments. To facilitate liquid handling, the top ITO glass was spin-coated with a hydrophobic layer (Teflon® AF 1600, DuPont, thickness 120 nm). The bottom black BT (Bismaleimide Triazine) resin plate with Cu driving electrodes patterns was covered with a dielectric layer. It was manufactured by Chip Win Technology Co., Ltd, Taiwan. A Teflon layer (thickness 120 nm) was also coated on the bottom plate to make the surface hydrophobic. Before assembly of the two plates, the liquids were manually pipetted on the bottom plate; the top plate was then carefully placed and adhered onto appropriate spacers (thickness 50 $\mu$m) attached to the bottom plate. The multiple driving electrodes on the bottom plate were individually activated through single pole double throw (SPDT) relays (LU-5, Rayex Electronics). The electric potential of the electrodes was switched between the electric ground and high potentials. AC electric signals with a frequency of 1 kHz were generated by a function generator (33210 A, Agilent Technologies) and amplified through an amplifier (A-304, A. A. Lab Systems). The relays were switched by the digital output signals of a data-acquisition device (USB-6509, National Instruments) programmed with LabVIEW software.

### 2.2. Fabrication of porous Bragg Microcavities

To incorporate the porous BM onto the EMF chip we proceeded to its deposition by PV-OAD on the desired driving electrode (from now on the BM-electrode) of the chip by covering the rest with an aluminum shadow mask. Simultaneously, deposition by electron beam evaporation was also performed on ITO substrates and on silicon wafers. As reported in previous works alternating layers were stack deposited by evaporation at a zenithal angle of deposition ($\alpha$) of 70° [36, 37]. The BM stack consisted of 15 alternating layers of $TiO_2$ and $SiO_2$, starting and ending with $TiO_2$, each of them with a thickness of about 85 nm except for the central layer that, acting as optical defect, had a thickness of ca. 200 nm.

### 2.3. Optical monitoring of the BM-electrode

Reflectance-visible spectra of the different parts of the device including the BM-electrode were taken using a home-made optical setup consisting of an extensive source of light (range 350–900 nm, Halogen Reflector Lamp Decostar Osram®) collimated to a spot of around 1 mm$^2$ and a camera connected to a computer with a detector

**Figure 1.** (a) Cross section scheme of the EMF device incorporating electrode and hydrophobic Teflon layers to facilitate the manipulation of liquids and light beam interrogation through the BM deposited onto one electrode. Note that the different parts of the chip are not plotted in the same scale. (b) Cross sectional SEM micrographs of the porous BM. A scheme of the stack indicating the composition of each layer, $TiO_2$ (green) or $SiO_2$ (orange) is overprinted onto the micrograph. (c) EMF device after depositing a BM onto a selected driving electrode (the BM-electrode). The green and blue squares are zoom views of this zone covered with the deposited BM taken without and with external illumination, respectively. (d) Visible reflectance spectra of selected zones of the chip: the BM-electrode zone, a driving electrode and the black background. The spectrum of a BM deposited onto a transparent ITO substrate is included as a reference.

placed in the center of the camera. The impinging and reflected beam directions were 20° apart (incidence 10° off normal). Spectra were recorded before and after infiltrating the BM with liquids either dripped manually with a pipette or moved to the BM-electrode by EWOD or DEP actuation. The room temperature during the experiments was 20 °C.

A silicon wafer covered with the BM was diced to take Scanning Electron Microscopy (SEM) cross section micrographs in a Hitachi S4800 field emission microscope working at 2 keV primary beam energy. Both detecting modes, Secondary Electron (SE) and Back Scattered Electron (BSE) were used to highlight either topographic or compositional information, respectively.

## 3. Results and discussion

### 3.1. Characterization of the BM deposited onto EMF device

Figure 1(b) shows SEM micrographs of the BM deposited onto a silicon wafer, together with an overprinted scheme of the layers stack. The BSE micrograph reveals the composition of each layer of the stack with the $TiO_2$ corresponding to the brighter layers and the $SiO_2$ to the darker ones. Meanwhile, the SEM micrograph shows the typical slanted nanocolumnar microstructure of the PVD-OAD films and highlights the high porosity of these layers that in previous works we have estimated around 50%. Figure 1(c) presents the EMF device with the BM deposited on a pre-selected driving electrode (the BM-electrode) that remained uncovered by the mask during deposition. This part presented an orange color that was taken as hint of the successful deposition of the BM,
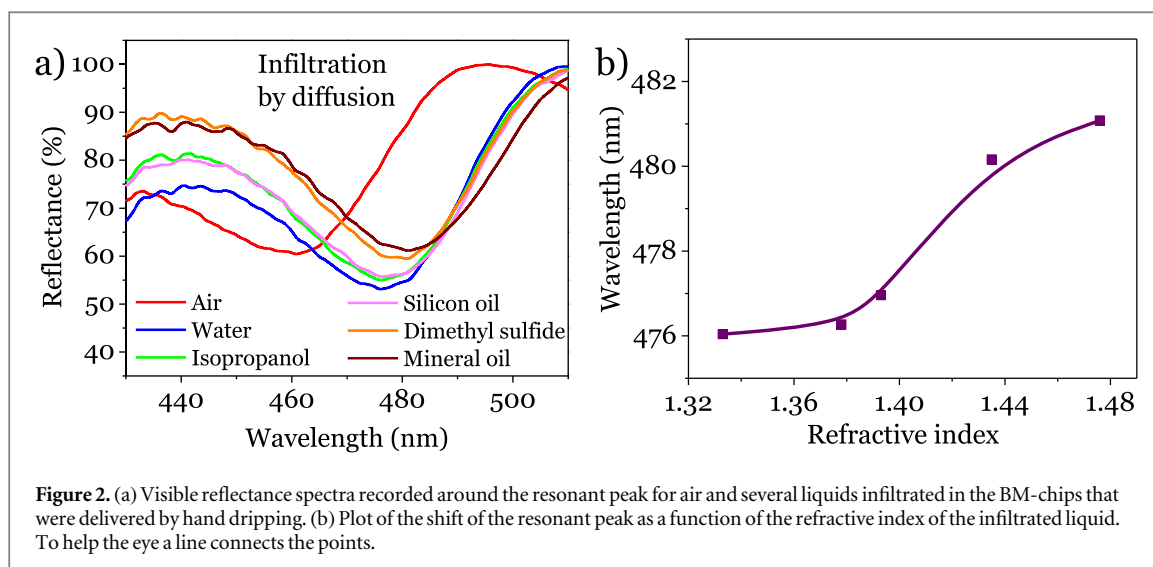
**Figure 2.** (a) Visible reflectance spectra recorded around the resonant peak for air and several liquids infiltrated in the BM-chips that were delivered by hand dripping. (b) Plot of the shift of the resonant peak as a function of the refractive index of the infiltrated liquid. To help the eye a line connects the points.

providing a straightforward way to localize it onto the device. An optical characterization of the different parts of the EMF device in the form of reflectance spectra is shown in figure 1(d), together with an equivalent spectrum of a reference BM sample deposited onto an ITO substrate which is included for comparison. This reference spectrum depicts the typical wide reflectance gap and resonance peak of this type of 1D photonic structure (blue line in Figure 1(d)). As reported in previous works [36–38], this resonant peak at around 460 nm can be used to monitor changes in the BM when it is liquid-infiltrated. The reflectance spectrum recorded for the BM deposited onto the EMF chip depicts a similar spectrum where the resonant peak was less well defined and appeared slightly shifted to shorter wavelengths (red line in Figure 1(d)). We attributed this slight loss of optical quality for the BM deposited onto the EMF device to the roughness of the driving electrode. Optical spectra of the black background and of a driving electrode of the EMF, also reported in Figure 1, were recorded to identify their possible contributions to the BM spectrum in case of misalignment of the incident beam. The high reflectivity of the BM-electrode zone in comparison with the black background and a driving electrode of the DMF device could be appreciated with the bare eyes in the dashed blue square of Figure 1(c) and was characterized by the spectrum presented in Figure 1(d).

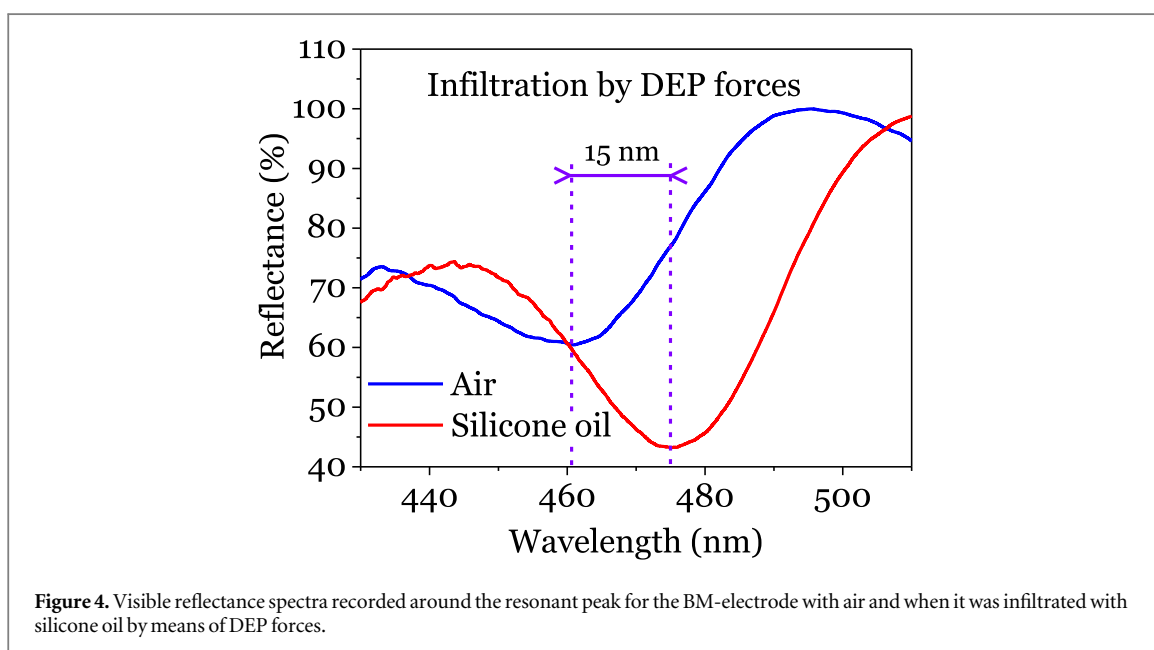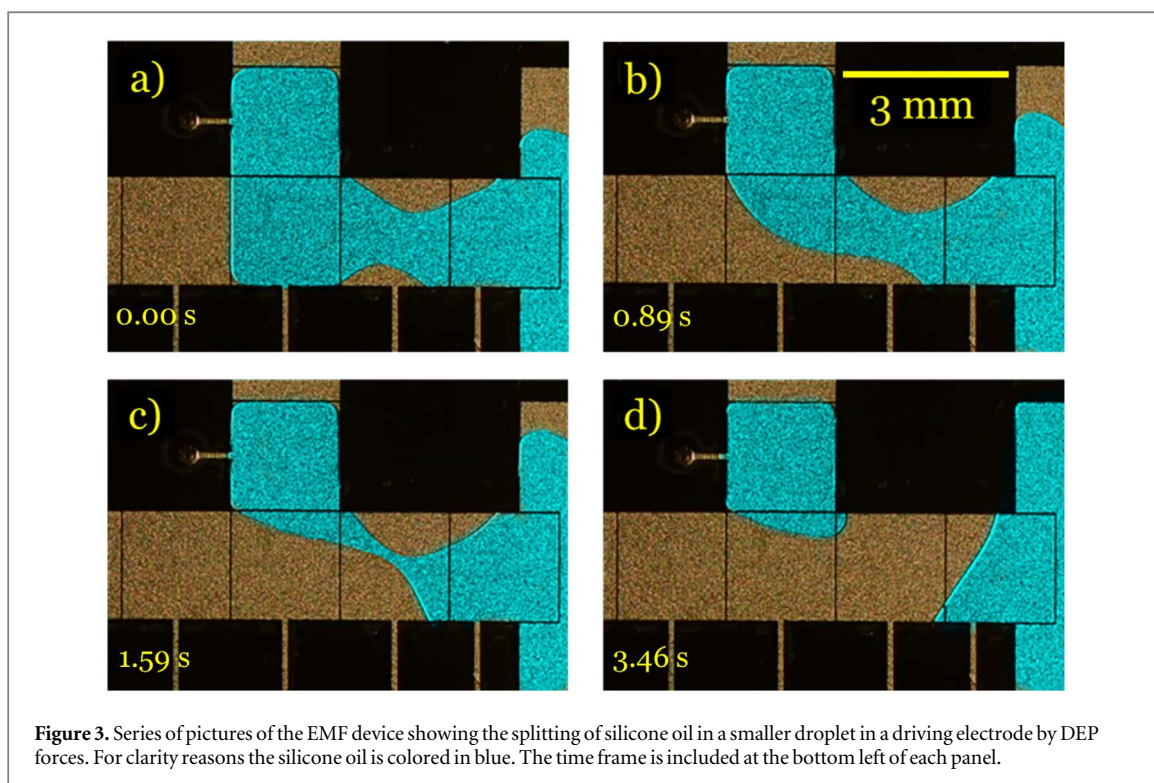### 3.2. Optofluidic response of the BM-EMF chip.
Figure 2 presents the optofluidic characterization of the BM-electrode when delivering the liquids directly onto the BM with a pipette. Dripping liquids onto this zone should fill the pores of the BM and, according to previous analysis, would induce changes in the optical response of the BM transducer [36–38], Effectively, Figure 2(a) shows that the infiltration with different liquids led to a shift of the optical spectra to larger wavelengths (i.e., a *redshift*), that in the case of mineral oil reached up to 21 nm. The representation of the magnitude of these shifts as a function of the refractive index of the infiltrating liquid in Figure 2(b) shows a clear dependence that can be used to differentiate a specific liquid from others with different refractive index. The plot shows that below a RI of 1.38 the accuracy of the sensor decreases preventing to discriminate liquids below this point.

### 3.3. Liquid movement in the EMF-device
Isopropanol (mainly driven by EWOD) and silicone oil (mainly driven by DEP) were used to determine the working parameters of the EMF device to move liquid droplets from one driving electrode to the other on the chip. Droplets of these liquids were moved by electrical actuation and the displacement from one electrode to another took around 0.2 s. A square wave signal of voltage 360 $V_{pp}$ and a frequency of 1 kHz were supplied to move the liquid droplets, as well as to split the liquid into small droplets of volume ~ 0.2 $\mu$l. A succession of pictures showing the formation of specific silicone oil patches in the EMF-device is presented in Figure 3.

### 3.4. Optofluidic response of the BM-electrode infiltrated with silicone oil by dielectrophoretic forces
Main objective of this work was to investigate the ability of liquid droplet manipulation on an EMF device incorporated with a liquid transducer. To that end, a big silicone oil droplet was split into smaller droplets and one of them was delivered to the BM-electrode by means of the DEP forces by electrical actuation on the device. Figure 4 is the optofluidic response of the BM-electrode showing that the resonant peak of the BM experienced the same redshift (i.e., 15 nm) as that found when dripping the silicone oil by a pipette (cf Figure 2). This evidence proved the successful integration of an optofluidic BM transducer onto the EMF device and the

**Figure 3.** Series of pictures of the EMF device showing the splitting of silicone oil in a smaller droplet in a driving electrode by DEP forces. For clarity reasons the silicone oil is colored in blue. The time frame is included at the bottom left of each panel.



**Figure 4.** Visible reflectance spectra recorded around the resonant peak for the BM-electrode with air and when it was infiltrated with silicone oil by means of DEP forces.

successful driving of liquid droplets by DEP actuation. These results showed that the porous BM has worked acceptably well in combination with the EMF optofluidic device and we attributed the lesser shift observed in comparison with the reference BM to some microstructural changes induced by the growth of the porous thin films on the Teflon coating covering the ITO layer of the EMF device.

## 4. Conclusions

In this work, an optofluidic device combining a porous thin film photonic structure on an EWOD/DEP-based EMF device is presented for the first time. For this aim, porous BMs have been successfully deposited onto one driving electrode of an EMF device. The thin film deposition process did not affect the electromicrofluidic features of the EMF device, an outstanding result that proves that optofluidic transducers and EMF systems can be integrated in a unique device. The optofluidic transducer preserved its performance when incorporated onto

the EMF device, as proved by manually delivering the liquid onto the sensing region and by electrical driving the liquid analyte droplet to the zone containing the BM. An additional advantage of integrating the BM into an EMF device is the lower volume needed for analysis in comparison with the amount required when using other rudimentary sample delivery systems.

## Acknowledgments

## ORCID iDs

Manuel Oliva-Ramírez ⓘ https://orcid.org/0000-0003-0249-377X
Víctor Rico-Gavira ⓘ https://orcid.org/0000-0002-5083-0390
Agustín R González-Elipe ⓘ https://orcid.org/0000-0002-6417-1437

## References

[1] Psaltis D, Quake S R and Yang C 2006 Developing optofluidic technology through the fusion of microfluidics and optics *Nature* **442** 381–6
[2] Eftekhari F, Escobedo C, Ferreira J, Duan X, Girotto E M, Brolo A G, Gordon R and Sinton D 2009 Nanoholes as nanochannels: flow-through plasmonic sensing *Anal. Chem.* **81** 4308–11
[3] Pang L, Hwang G M, Slutsky B and Fainman Y 2007 Spectral sensitivity of two-dimensional nanohole array surface plasmon polariton resonance sensor *Appl. Phys. Lett.* **91** 123112
[4] Yang J-C, Ji J, Hogle J M and Larson D N 2008 Metallic nanohole arrays on fluoropolymer substrates as small label-free real-time bioprobes *Nano Lett.* **8** 2718–24
[5] Im H, Lesuffleur A, Lindquist N C and Oh S-H 2009 Plasmonic nanoholes in a multichannel microarray format for parallel kinetic assays and differential sensing *Anal. Chem.* **81** 2854–9
[6] Yanik A A, Huang M, Artar A, Chang T-Y and Altug H 2010 Integrated nanoplasmonic-nanofluidic biosensors with targeted delivery of analytes *Appl. Phys. Lett.* **96** 021101
[7] Zangooie S, Jansson R and Arwin H 1998 Reversible and irreversible control of optical properties of porous silicon superlattices by thermal oxidation, vapor adsorption, and liquid penetration *J. Vac. Sci. Technol. A* **16** 2901–12
[8] Nishijima Y, Ueno K, Juodkazis S, Mizeikis V, Misawa H, Tanimura T and Maeda K 2007 Inverse silica opal photonic crystals for optical sensing applications *Opt. Express* **15** 12979–88
[9] Dorfner D F, Hürlimann T, Zabel T, Frandsen L H, Abstreiter G and Finley J J 2008 Silicon photonic crystal nanostructures for refractive index sensing *Appl. Phys. Lett.* **93** 181103
[10] Hasek T, Kurt H, Citrin D S and Koch M 2006 Photonic crystals for fluid sensing in the subterahertz range *Appl. Phys. Lett.* **89** 173508
[11] Casquel R, Soler J A, Holgado M, López A, Lavín A, de Vicente J, Sanza F J, Laguna M F, Bañuls M J and Puchades R 2015 Sub-micrometric reflectometry for localized label-free biosensing *Opt. Express* **23** 12544
[12] Rindorf L, Jensen J B, Dufva M, Pedersen L H, Høiby P E and Bang O 2006 Photonic crystal fiber long-period gratings for biochemical sensing *Opt. Express* **14** 8224–31
[13] Fan X and White I M 2011 Optofluidic microsystems for chemical and biological analysis *Nat. Photonics* **5** 591–7
[14] Mugele F and Baret J-C 2005 Electrowetting: from basics to applications *J. Phys. Condens. Matter* **17** R705–74
[15] Fan S-K and Wang F-M 2014 Multiphase optofluidics on an electro-microfluidic platform powered by electrowetting and dielectrophoresis *Lab Chip* **14** 2728–38
[16] Fan S-K, Hsieh T-H and Lin D-Y 2009 General digital microfluidic platform manipulating dielectric and conductive droplets by dielectrophoresis and electrowetting *Lab Chip* **9** 1236–42
[17] Fan S-K, Hsu Y-W and Chen C-H 2011 Encapsulated droplets with metered and removable oil shells by electrowetting and dielectrophoresis *Lab Chip* **11** 2500–8
[18] Chiang M-Y, Hsu Y-W, Hsieh H-Y, Chen S-Y and Fan S-K 2016 Constructing 3D heterogeneous hydrogels from electrically manipulated prepolymer droplets and crosslinked microgels *Sci. Adv.* **2** e1600964
[19] Fan S-K, Shen Y-T, Tsai L-P, Hsu C-C, Ko F-H and Cheng Y-T 2012 Atmospheric-pressure microplasma in dielectrophoresis-driven bubbles for optical emission spectroscopy *Lab Chip* **12** 3694–9
[20] Ahmadi A, Devlin K D, Najjaran H, Holzman J F and Hoorfar M 2010 *In situ* characterization of microdroplet interfacial properties in digital microfluidic systems *Lab Chip* **10** 1429–35
[21] Campbell C T and Kim G 2007 SPR microscopy and its applications to high-throughput analyses of biomolecular binding events and their kinetics *Biomaterials* **28** 2380–92
[22] Slavík R, Homola J and Čtyroký J 1998 Miniaturization of fiber optic surface plasmon resonance sensor *Sens. Actuators B Chem.* **51** 311–5
[23] Homola J 2008 Surface plasmon resonance sensors for detection of chemical and biological species *Chem. Rev.* **108** 462–93
[24] Liu Y, Liu Q, Chen S, Cheng F, Wang H and Peng W 2015 Surface plasmon resonance biosensor based on smart phone platforms *Sci. Rep.* **5** 12864
[25] Caucheteur C, Guo T and Albert J 2015 Review of plasmonic fiber optic biochemical sensors: improving the limit of detection *Anal. Bioanal. Chem.* **407** 3883–97

[26] Jin G, Unfricht D W, Fernandez S M and Lynes M A 2006 Cytometry on a chip: Cellular phenotypic and functional analysis using grating-coupled surface plasmon resonance *Biosens. Bioelectron.* **22** 200–6

[27] Singh B K and Hillier A C 2006 Surface plasmon resonance imaging of biomolecular interactions on a grating-based sensor array *Anal. Chem.* **78** 2009–18

[28] Fu Q and Sun W 2001 Mie theory for light scattering by a spherical particle in an absorbing medium *Appl. Opt.* **40** 1354–61

[29] Jain P K, Lee K S, El-Sayed I H and El-Sayed M A 2006 Calculated absorption and scattering properties of gold nanoparticles of different size, shape, and composition: applications in biological imaging and biomedicine *J. Phys. Chem. B* **110** 7238–48

[30] Wang D-S and Fan S-K 2016 Microfluidic surface plasmon resonance sensors: from principles to point-of-care applications *Sensors* **16** 1175

[31] Malic L, Veres T and Tabrizian M 2009 Two-dimensional droplet-based surface plasmon resonance imaging using electrowetting-on-dielectric microfluidics *Lab Chip* **9** 473–5

[32] Ceyssens F, Witters D, Van Grimbergen T, Knez K, Lammertyn J and Puers R 2013 Integrating optical waveguides in electrowetting-on-dielectric digital microfluidic chips *Sens. Actuators B Chem.* **181** 166–71

[33] Luan L, Evans R D, Schwinn D, Fair R B and Jokerst N M 2008 Chip scale integration of optical microresonator sensors with digital microfludics systems *LEOS 2008–21st Annu. Meet. IEEE Lasers Electro-Opt. Soc.* pp 259–60

[34] Luan L, Royal M W, Evans R, Fair R B and Jokerst N M 2012 Chip scale optical microresonator sensors integrated with embedded thin film photodetectors on electrowetting digital microfluidics platforms *IEEE Sens. J.* **12** 1794–800

[35] Arce C L, Witters D, Puers R, Lammertyn J and Bienstman P 2012 Silicon photonic sensors incorporated in a digital microfluidic system *Anal. Bioanal. Chem.* **404** 2887–94

[36] Oliva-Ramirez M, González-García L, Parra-Barranco J, Yubero F, Barranco A and González-Elipe A R 2013 Liquids analysis with optofluidic bragg microcavities *ACS Appl. Mater. Interfaces* **5** 6743–50

[37] Oliva-Ramirez M, Barranco A, Löffler M, Yubero F and González-Elipe A R 2015 Optofluidic modulation of self-associated nanostructural units forming planar bragg microcavities *ACS Nano.* **10** 1256−1264

[38] Oliva-Ramírez M, Gil-Rostra J, Yubero F and González-Elipe A R 2018 Robust polarization active nanostructured 1D Bragg Microcavities as optofluidic label-free refractive index sensor *Sens. Actuators B Chem.* **256** 590–9

[39] Granqvist C G and Hultåker A 2002 Transparent and conducting ITO films: new developments and applications *Thin Solid Films* **411** 1–5